Analytica Chimica Acta 1058 (2019) 89–96

Contents lists available at ScienceDirect

Analytica Chimica Acta

journal homepage: www.elsevier.com/locate/aca

Hierarchical assembled nanomaterial paper based analytical devices for simultaneously electrochemical detection of microRNAs

Rong Tian [a, b, c, *], Yujing Li [d], Jingwei Bai [a, **]

[a] School of Pharmaceutical Sciences, Tsinghua University, Beijing, 100084, China
[b] Tsinghua-Peking Joint Center for Life Sciences, Beijing, 100084, China
[c] Chongqing Institute of Green and Intelligent Technology, Chinese Academy of Sciences, China
[d] Material Institute, Beijing Institute of Technology, Beijing, 100081, China

HIGHLIGHTS

- MoS_2/AuNPs/AgNW paper-based electrode was used as sensing platform.
- Hairpin DNA nanostructures-based biosensor was developed with the detection limit of 0.1 fM.
- PtCuMOFs/DNA was used for simultaneous detection miRNA and signal amplification.
- The DNA biosensor could be utilized in real serum sample analysis.

ARTICLE INFO

Article history:
Received 8 September 2018
Received in revised form
28 December 2018
Accepted 24 January 2019
Available online 29 January 2019

Keywords:
Paper device
MOFs
MicroRNA
Simultaneous detection

ABSTRACT

Paper based biosensor devices have the benefit of easy-use, low-cost and environmental friendly for point-of-care diagnostic application. In this research, we report a novel form of paper based biosensor with hierarchical assembled nanomaterials and MOF enhanced bio-probes for the simultaneous detection of microRNA-141 (miR-141) and microRNA-21 (miR-21) which have the potential for early cancer detection. The combination of multi-dimensional nanomaterial allows low impedance and high sensing area on typical poorly defined paper substrate. MOF conjugated bio-probe, methylene blue (MB) and ferrocene (Fc) with distinguishable electrochemical signal, further contributed to the high selectivity and sensitivity. Simultaneously detection of miR-141 and miR-21 with a detection limit of 0.1 fM was demonstrated under optimal conditions. All these features enable accurately target detection in serum samples. Therefore, this strategy is of promising as an inexpensive, easy access diagnosis platform for cancers by means of simultaneously detection of a variety of miRNA biomarkers.

1. Introduction

MicroRNAs (miRNAs) are noncoding RNA which has a length of 21–23 nucleotides that play a major role in control of gene expression by repressing protein synthesis at the post-transcriptional level [1]. Aberrant miRNA expression is directly associated with various pathological diseases such as cancer, cardiovascular disease and neurological disorders. Specifically, the detection of miRNA is crucial to early cancer diagnose [2]. The analysis of miRNA is challenging because their short lengths, low levels in body fluid, and a high degree of sequence homology. Nevertheless, several methods have been developed for miRNA analysis, including microarrays, electrocatalysis and northern blotting [3,4]. However, these techniques suffer from low sensitivity and time-consuming operation. Electrochemical analytic technique is attractive for miRNA detection due to cost effectiveness, simplicity and easy of miniaturization. Yao et al. developed a simple, label-free for detection of miRNA-24 by monitoring the oxidation signal of guanine on multi-walled carbon nanotubes (MWCNTs) based electrochemical electrodes [5]. Zheng et al. proposed an sensitive miRNA detection strategy by ingeniously combining the target-catalyzed hairpin assembly (CHA) and supersandwich amplification [6]. Zou et al. presented a label-free and PCR-free electrochemical method for multiplexed evaluation

* Corresponding author. School of Pharmaceutical Sciences, Tsinghua University, Beijing, 100084, China.
** Corresponding author.
E-mail addresses: rtian2017@tsinghua.edu.cn (R. Tian), jingwbai@mail.tsinghua.edu.cn (J. Bai).

https://doi.org/10.1016/j.aca.2019.01.036
0003-2670/

of miRNA targets in single-tube [7]. Despite these advantage of sensor platform on exotic electrode materials, enabling sensitive and reliable detection of miRNA on low-cost electrochemical platform may exert true impact on in-vitro diagnosis.

Paper-based analytical devices with unique features such as low cost, lightweight and flexible nature have attracted much attention for bio-analytical point-of-care (POC) platform [8,9]. The porous nature of paper substrate may also enable excellent detection limit due to large surface are to immobilize sensing materials [10–12]. To date, the analytical methods of various paper-based devices are primarily utilized for the qualitative detection of biomarkers. Wendell et al. described for the first time the 3D printing fabrication of paper-based enzymatic reactors (PERs) and electrochemical glucose detection in artificial serum sample [13]. Yan et al. fabricated a simple and novel FLS-enhanced fluorescence/visual bimodal biosensor for multiplexed detections of various biomarkers with low fluorescence background and high sensitivity [14]. Zhang et al. describe a complementary quantitative point-of-care assay based on Rubik's Cube (RC) platform [15].

In addition, two-dimensional (2D) nanomaterials have been of much interest to improve the performance of various sensor platform due to their unique properties such as excellent mechanical strength, large surface-volume ratio, enhanced catalytic activity and unique electrical properties [16,17]. Especially, 2D molybdenum sulfide (MoS_2) decorated with gold nanoparticles (AuNPs) for electrochemical sensory application enabling large activated surface as well as superior electron transfer efficiency [18–26]. Metal-organic frameworks (MOFs), on the other hand, as a new class of porous materials offering inherent large surface areas, tunable pore sizes and tailorable chemistry [27–29], can be potentially used as host matrix material to anchor large amount of sensory reagent, such as hemin for electrochemical detecting hydrogen peroxide (H_2O_2) [30,31].

In this work, we developed a simple filtration based strategy to fabricate paper based biosensor with hierarchically assembled nanomaterial composites to simultaneously detect two types of miRNAs(Fig. 1). Compared with the previously reported electrochemical sensory constructions, our proposed paper based biosensor possessed two major advantages: (1) paper based substrate enable filtration methods to efficient assemble different functional components with relatively low fabrication cost; (2) hierarchically assembled nanomaterials operated coordinately can reach the optimal sensory performance even on poorly conditioned paper substrate. The first layer silver nanowire is designed to support the conductivity of paper-based electrode; second layer MoS_2/AuNPs provides large surface area for anchoring capturing oligos and providing conducting pathway for electrochemical current. PtCuMOFs were chosen as the sink materials for secondary sensory probe to further enhance the electrochemical signal. With all these unique properties, we report one of the best sensing performance amount paper based electrochemical biosensor which can be directly comparable to other electrochemical sensor on exotic electrode substrate.

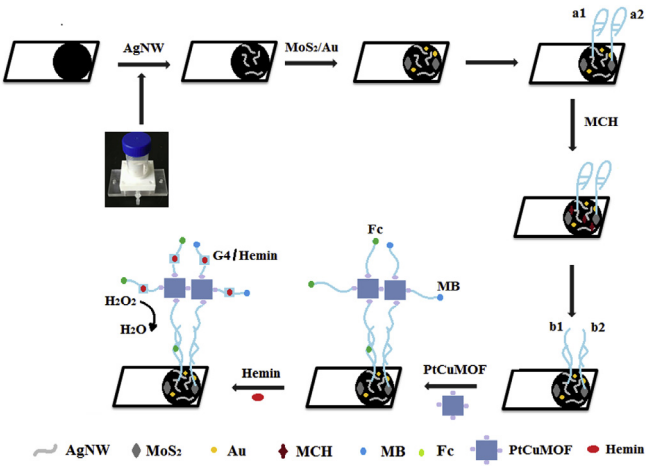

Fig. 1. Schematic diagram for the electrochemical detection.

2. Materials and methods

2.1. Chemical and oligos

Polyvinylpyrrolidone (PVP), sodium borohydride ($NaBH_4$), copper nitrate-trihydrate ($Cu(NO_3)_2 \cdot 3H_2O$), N, *N*-dimethylformamide (DMF), 2-amino terephthalic acid (NH_2-H_2BDC), chloroauric acid hydrated ($HAuCl_4 \cdot 4H_2O$) and chloroplatinic acid (H_2PtCl_6) were purchased from J & K Chemical Technology (Beijing, China). 6-Mercapto-1-hexanol (MCH), potassium ferricyanide ($K_3[Fe(CN)_6]$), potassium ferrocyanide ($K_4[Fe(CN)_6]$) and potassium chloride (KCl) were obtained from Linfeng Chemical Reagent Co., Ltd (Shanghai, China). MoS_2 nanosheet solution (1 mg L^{-1}) was provided by XFNANO Materials Tech Co., Ltd. (Nanjing, China). DNA immobilization buffer (300 mM NaCl, 25 mM tris-acetate, pH 8.0) and the supporting electrolyte phosphate buffer saline (PBS, 0.1 M) were made with miliQ water. All reagents were of analytical grade and used without further purification. DNA and miRNA sequences were synthesized by Sangon Biological Engineering Technology Co. Ltd. (Shanghai, China) and the detailed oligonucleotide sequences were listed in Table 1.

2.2. Instrument and characterizations

Electrochemical measurements including cyclic voltammetry (CV), electrochemical impedance spectroscopy (EIS) and Square Wave Voltammetry (SWV) were carried out with CHI 660E electrochemistry workstation (Shanghai Chenhua Instruments Co., Ltd., China). The paper electrode was cut into 1 cm × 3 cm in size, and Kapton tape was used to protect 1 cm × 2 cm area from one end of the paper and leave 1 cm × 1 cm for the sensory area. The paper electrode was wired out from the Kapton protecting side by elargol. A three-electrode setup was carried out for electrochemical test: the paper electrode as the working electrode with effective area of 1 cm × 1 cm, an Ag/AgCl (3.0 M KCl) reference electrode and a platinum wire counter electrode in the supporting electrolyte phosphate buffer saline (PBS). The morphology of filter paper, AgNW, MoS_2/AuNPs/AgNW, CuMOFs and PtCuMOFs were studied by Transmission Electron Microscopy(TEM)(Hitachi, HT7700), and Scanning Electron Microscopy (SEM) (Quanta 400 FEG, FEI, USA) equipped with Apollo 40 SDD X-ray Energy Dispersive Spectrometer (EDS). The UV–vis absorption spectra of CuMOFs and PtCuMOFs was recorded using a UV–vis spectrophotometer (Hitachi, U-3010). The powder X-ray diffraction (XRD) characterization was performed on PtCuMOFs using X-ray diffraction (Bruker, D8 Focus, Karlsruhe, Germany) with Cu K radiation at room temperature.

2.3. Synthesis of MOF materials

CuMOFs were synthesized based on previously reported method [32]. Typically, 0.40 g of PVP was dissolved in a mixture solution of 8 mL DMF and 8 mL ethanol under stirring, followed by adding 8 mL DMF containing 10.86 mg NH_2-H_2BDC and 36.24 mg $Cu(NO_3)_2$. After ultrasonicating for 25 min, the resultant mixture was transferred into a Teflon-lined autoclave container and kept at 100 °C for 5 h.

Table 1
Synthetic sequences used in the experiments.

Name	Sequence (5′-3′)
DNA1	HS-$(CH_2)_6$-CATACTCGAGCAGTCTACCATCTTTACCAGACAGTGTTATAGACTGC
DNA2	HS-$(CH_2)_6$-CTACATGGACCGTTCTATCAACATCAGTCTGATAAGCTATAGAACGG
miR-141	UAACACUGUCUGGUAAAGAUGG
miR-21	UAGCUUAUCAGACUGAUGUUGA
DNA3	HS-$(CH_2)_6$-TCAGACACGCAGTCTAGGGTAGGGCGGGTTGGGA-MB
DNA4	HS-$(CH_2)_6$-TCAGACACCCGTTCTA GGGTAGGGCGGGTTGGGA-Fc

The collected product by centrifugation at 5000 rpm was heated by adding 40 mL DMF at 100 °C for 12 h. To decorate the CuMOFs with PtNPs, 2 mL of 2 mM $NaBH_4$ and 200 μL of 1% H_2PtCl_6 were dropwisely added into the above CuMOFs solution and stirred for 1 h. The product was then collected by centrifugation at 10,000 rpm, and the precipitation was re-dispersed in 4 mL DI water for further use. The oligo functionalized was done by mixing 1 mL of PtCuMOFs product (1 mg mL^{-1}) with 100 μL of DNA3 or DNA4 solution (2 μM) for 12 h, and purified by three time centrifugation and ultra-pure water wash. The final products were dispersed in 2 mL of hybridization buffer (pH 7.4) and stored at 4 °C before use.

2.4. Preparation of sensory electrodes

The AuNPs were prepared as described in the literature [33]. In brief, sodium citrate (1.5 mL, 10 mg mL^{-1}) was added to the aqueous solution (100 mL) containing $HAuCl_4$ (1 wt%, 1 mL). Then, the mixture was heated to reflux and kept for 15 min. A wine red solution of AuNPs was obtained after being cooled to room temperature and stored at 4 °C. AgNWs with diameter about 80 nm and length about 10 μm were synthesized by reducing silver nitrate in the presence of Poly (vinylpyrrolidone) (PVP) in ethylene glycol [34]. Briefly, 32 g of $FeCl_3$ solution, 2 g of silver nitrate, and 2 g of PVP were added to 250 g of ethylene glycol. After the mixture was heated at 150 °C for 1.5 h, the reacted suspension was filtered through a cellulose acetate membrane filter, and redispersed in 60 mL of ethanol for further use. To build the paper electrode, filter paper was chosen as the paper substrate without prior treatment. With a house built vacuum apparatus, the AgNWs solution was slowly pump through the filtered paper in order to assemble the AgNWs on top. Then, Kapton tape is used to define the sensing area as described above. Next, 1 mg mL^{-1} of 100 μL MoS_2 and 100 μL AuNPs were sequentially filtered onto the predefine 1 cm^2 paper area. For capturing oligo functionalization, as prepared paper electrode was incubated in 6 μM hairpin DNA probes at 37 °C for 12 h in a homo-thermal water bath chamber, and washed with mili-Q water. After MCH blocking the non-specific absorption, the different concentrations of 10 μL miR-141 and 10 μL miR-21 were dropped on paper electrode, kept at 37 °C for 1 h and washed off by PBS. The electrochemical signals were generated by following steps: 10 μL of PtCuMOFs/DNA3 and PtCuMOFs/DNA4 were dropped onto the miRNA sample treated paper electrode and reacted at 37 °C for 2 h, followed by addition of hemin to form G-quadruplex structure (G4) for catalyzing H_2O_2. The PtCuMOFs/DNA3 and PtCuMOFs/DNA4 probe for miR-141 and miR-21 response differently due to the MB and Fc conjugation, which can be distinguished under different oxidation/reduction potential. Based on above process, our design can be used to quantitatively detect the two targets simultaneously.

3. Results and discussion

3.1. Characterization and functionalization of hierarchical assembled nanomaterial electrodes

The morphologies of the MoS_2/AuNPs/AgNW paper-based electrodes were characterized by scanning electron microscopy (SEM). The basic framework of bare filtered paper was shown to have cellulose fibers tightly stacked and intertwined with each other, as revealed in Fig. 2A. After filtering of 100 μL AgNW solution through the nanowires, with length of 10–20 μm and diameter of

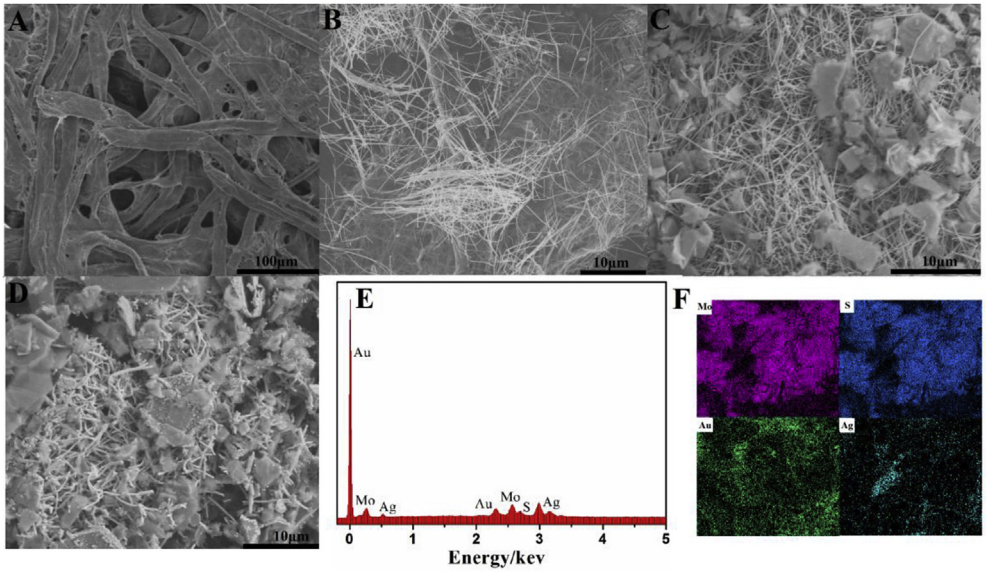

Fig. 2. SEM images of filter paper (A), AgNW (B), MoS_2/AgNW (C), MoS_2/AuNPs/AgNW (D), EDS pattern of MoS_2/AuNPs/AgNW (E) and SEM-EDX maps (F) in Mo Lα1, S Kα1, Au Mα1 and Ag Lα1 signals.

~70 nm formed well interconnected network on the top surface cellulose fibers framework to support the electrical conductive pathway (Fig. 2B). In the next step, 100 μL MoS_2 (2 mg mL^{-1}) and 100 μL AuNPs of 10 nm in size were filtered through the Ag-paper substrate to support the grafting of capturing primer oligo, as indicated by the SEM morphology and elemental analysis (Fig. 2C and D). The additional of MoS_2 provides larger surface area to capture more AuNPs, thus increase the miRNA capturing efficiency. Elemental analysis of the MoS_2/AuNPs/AgNW paper electrode was conducted by EDS and SEM-EDX mapping technique, as shown in Fig. 2E and F, implying the successful construction of multilayered MoS_2/AuNPs/AgNW hierarchical assembly. The structure of MoS_2/AuNPs was characterized using XRD (Fig. S1A).

After binding with target miRNA, PtCuMOFs were used as carrier for secondary capturing oligo and the sink for the electrochemical activator molecule. The synthesized CuMOFs is of 5 μm in size and cubic like morphology with 2 rounded corner (Fig. 3A). After PtNPs functionalized, a large amount of bright dots appeared on the surface of the CuMOFs (Fig. 3B), indicating the success attachment of PtNPs. The powder XRD patterns of the main diffraction peaks at 10.52°, 13.30°, 19.48°, 21.08°, 24.76°, 33.78°, 39.75°and 46.23°can be indexed to the lattice planes of Cu(−110), Cu(020), Cu(−211), Cu(202), Cu(222), Cu(400), Pt(111), Pt(200), which were in good agreement with those reported in literature (Fig. 3C) [35,36]. The UV−vis absorption spectrum of the CuMOFs (curve a) and PtCuMOFs (curve b) also confirm the formation of PtNPs with an absorption peak at 375 nm (Fig. 3D) [37]. Therefore, we can safely make a conclusion that PtNPs were successfully doped into the synthesized nanocomposites. The FT-IR spectra of PtCuMOFs/DNA4 and PtCuMOFs/DNA3 was characterized in Fig. S1B.

3.2. Electrochemical performance of the paper electrode

We compare AgNW, MoS_2/AgNW with MoS_2/AuNPs/AgNW paper electrode by CV in a 2 mM $[Fe(CN)_6]^{3-/4-}$ solution (Fig. S2A) and Electrode surface modification without PtCuMOFs and with PtCuMOFs is characterized by SWV (Fig. S2B). The functionalization of the MoS_2/AuNPs/AgNW paper electrode with DNA oligos and so the sensory performance was firstly evaluated by CV measurement in a 2 mM $[Fe(CN)_6]^{3-/4-}$ solution. As shown in Fig. 4A, a pair of typical reversible redox peaks are observed (curve a), corresponding to the redox potential of $[Fe(CN)_6]^{3-/4-}$. After functionalization with hairpin DNA(curve b), the redox peak value decreased, which can be attributed to the binding of negative charged capture probe DNA which reduced the flux of the negatively charged $[Fe(CN)_6]^{3-/4-}$ to the electrode surface by electrostatic repulsion as well as the steric hindrance. Due to the similar effect, the peak current reduced further after hybridize with MCH blocking remaining electrochemical active sites(curve c), and so does the target miRNA (curve d). In order to amplify the electrochemical sensing signal, CuMOFs particle with decorated PtNPs was used as carriers to attach the secondary capture oligo DNA3 and DNA4. When PtCuMOFs/DNA hybridize with miRNA, the $[Fe(CN)_6]^{3-/4-}$ redox peak value further decreased (curve e), indicating the formation of multistacked sensing structure [38]. EIS characterization also confirmed the formation of hierarchically assembled structure, as the R_{ct} value increases from 1250 Ω to 3100 Ω step by step after the immobilization of hairpin DNA(curve b), MCH blocking(curve c), miRNA hybridization (curve d) and PtCuMOFs binding (curve e) (Fig. 4B).

3.3. Optimization of the experimental parameters for the sensory performance

The interaction of bioanalyte with sensory surface is typically affected by physical parameters such as temperature, interaction time and density of surface activation sites which in our case revealed by the amount of the surface capture probe. To reach the most favorable sensing performance, both the reaction

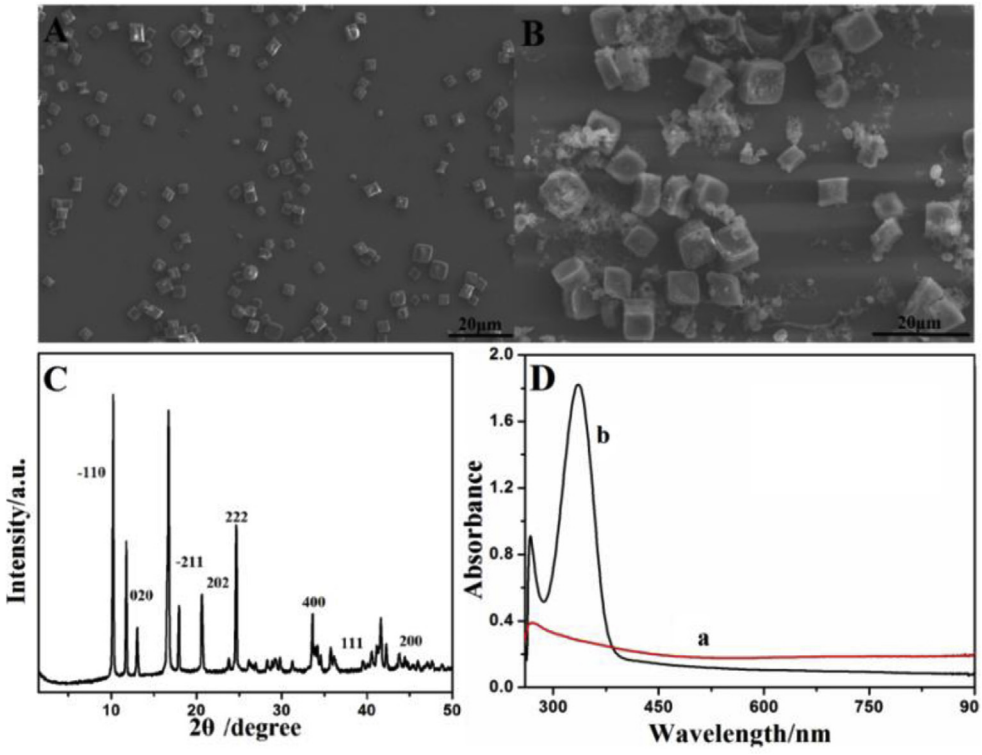

Fig. 3. SEM images of (A) CuMOFs and (B) PtCuMOFs, (C) XRD patterns of PtCuMOFs, (D) UV−Vis absorption spectra of CuMOFs(a) and PtCuMOFs(b).

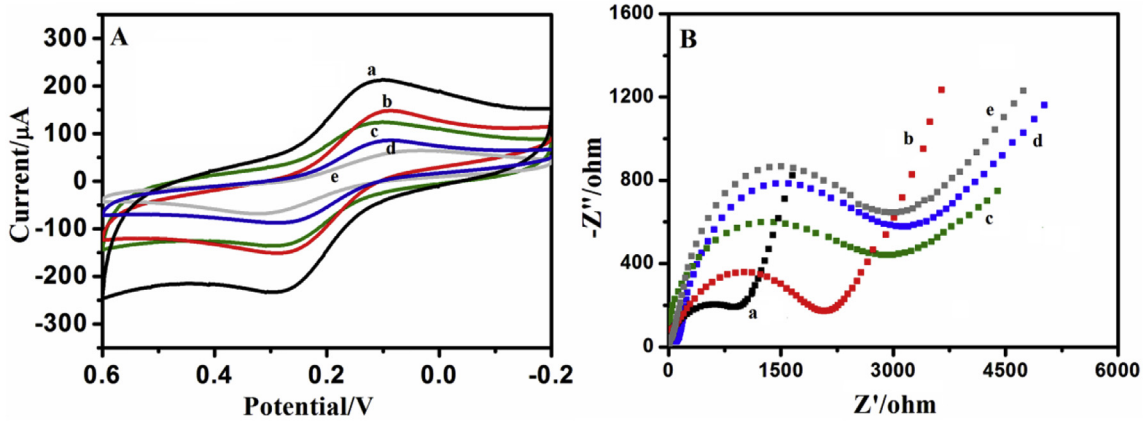

Fig. 4. (A) CVs, (B) EIS recorded at MoS_2/AuNPs/AgNW(a), hairpin DNA(b), MCH(c), miRNA (d) and PtCuMOFs/DNA(e) modified electrodes in 2 mM $Fe(CN)_6^{3-/4-}$ containing 0.1 M KCl solution at a scan rate of 100 mV s^{-1}.

temperature and time were optimized.

3.3.1. The temperature

The interaction temperature of PtCuMOFs/DNA3 and PtCuMOFs/DNA4 probe with miR-141(curve b) and miR-21 (curve a) was investigated from 20 to 50 °C with the addition of 1 nM target molecule. As shown in Fig. 5A, the redox current of both MB and Fc increased with temperature owing to the improved ion mobility, and reached a maximum at 37 °C. The redox current declined after 37 °C may be attributed to the dehybridization effect of target miRNA at higher temperature. Therefore, 37 °C was chosen as the optimal temperature to maximize the sensory performance.

3.3.2. The incubation time of miRNA

At this chosen temperature, the shortest time to reach the optimum interaction for miRNA with capture probe was also investigated. As illustrated in Fig. 5B, the electrochemical response increased with extending the hybridization time from 1 h to 2 h, and reached the plateau after that. Therefore, we believe the incubation time of 2 h is enough to achieve the hybridization

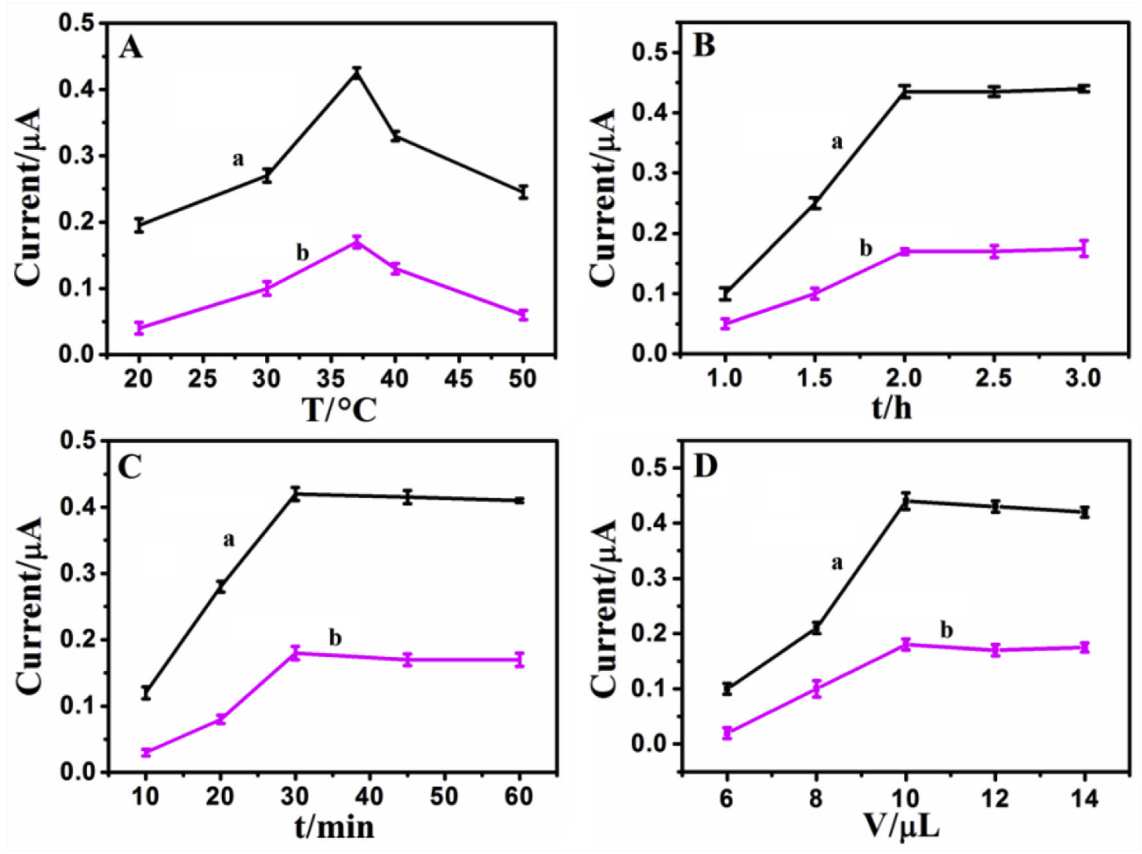

Fig. 5. (A) The temperature, (B) the incubation time of miRNA, (C) the reaction time of hemin and (D) the effect of PtCuMOFs/DNA loading with 1 nM miR-141(curve b) and 1 nM miR-21(curve a).

equilibrium between target miR-141(curve b), miR-21 (curve a) and capture DNA probe.

3.3.3. The reaction time of hemin

The interaction time of G4 with hemin was also studied in the range of 10–60 min with the addition of 1 nM miR-141(curve b) and 1 nM miR-21(curve a). As in Fig. 5C, the current response of MB and Fc increased with interaction time, and tended to level off after 30 min of incubation. For most of the following sensory experiment, 30 min was sufficient to reach high redox current.

3.3.4. The effect of PtCuMOFs/DNA loading

Lastly, to obtain high detection sensitivity, the surface loading of probe PtCuMOFs/DNA loading was optimized. As shown in Fig. 5D, the electrochemical response enhanced with increasing the probe PtCuMOFs/DNA loading from 6 to 14 μL for both case of MB and Fc, and reached a plateau with slightly reduction after 10 μL addition which might due to the overloading of enhancer complex block the diffusion of the electrochemical reactive molecules.

3.4. MicroRNA sensing performance

The sensing strategy of our experiment is as following: the target miRNA is captured with DNA1 and DNA2 immobilized on the MoS_2/AuNPs/AgNW paper electrode surface; then, PtCuMOFs/DNA3 and PtCuMOFs/DNA4 reporter probes are hybridized to the captured miRNA on electrode surface and generate faradaic current with conjugated MB and Fc. The concentration of miR-141 and miR-21 are reflected by the amount of PtCuMOFs/DNA1 and PtCuMOFs/DNA2 complex hybridized and measured by electrochemical signal of MB (potential at −0.05 V) and Fc (potential at 0.4 V) respectively. Thus, our design can be used to quantitatively measure the two targets simultaneously. With a series dilution of miR-141 and miR-21 in DEPC, the currents value of MB and Fc increased with the concentration of miR-141 and miR-21 varied from 1 fM to 1 nM, with the lowest detection limit (LOD) calculated to be 0.1 fM (S/N = 3)(Fig. 6A). As shown in Fig. 6B and C, the sensory current values fit linearly with the logarithm of target miRNA concentrations over a wide concentration region with a relative coefficient of 0.995 for miR-141, and 0.991 for miR-21. The high sensitivity of the sensor might be attributed to the use of PtCuMOFs as efficient electrochemical signal amplifier, supported by large amount of redox probe DNA loading as well as the PtNPs of peroxidase-like activity. As a result, the trace binding of target miRNA will link to gigantic PtCuMOFs particle entity with numerous catalytic center which in turn, cause the significant enhancement of the signal readout.

The expected detection limit as low as 0.1 fM by our strategy is amount the lowest for miR-141 and miR-21 detection comparing to other reported value (Table 2). Furthermore, our proposed method based on low cost, flexible and easy fabrication paper substrate, provides a foundation for high performance, low cost POC type of electrochemical sensor application.

3.5. Specificity, stability and reproducibility

For practical application, it is necessary evaluate the sensory performance for its specificity, stability, reproducibility, etc. The specificity is typically accessed by its anti-interference capability against miRNA sequence with high similarity such as miR-210 and

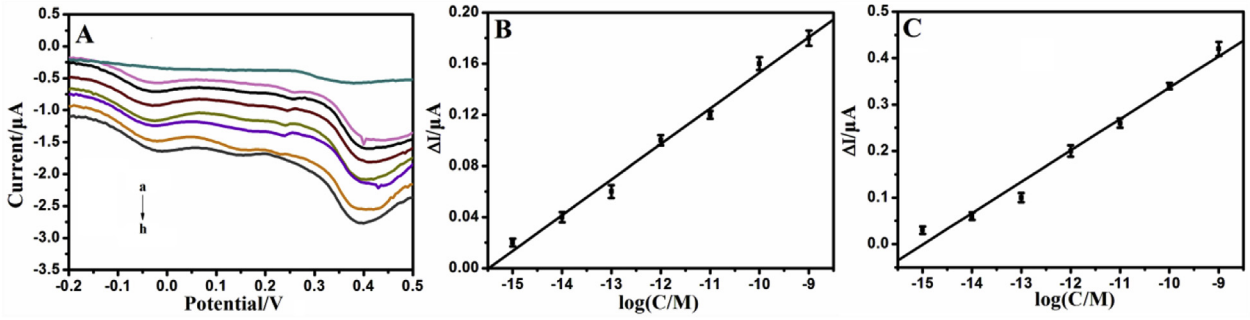

Fig. 6. (A) The SWVs of the proposed assay in the presence of different concentrations of miR-141 and miR-21 from a to h (0, 10^{-15},10^{-14}, 10^{-13}, 10^{-12}, 10^{-11}, 10^{-10} to 10^{-9} M); (B) The calibration plot in the presence of different concentrations of miR-141; (C) The calibration plot in the presence of different concentrations of miR-21.

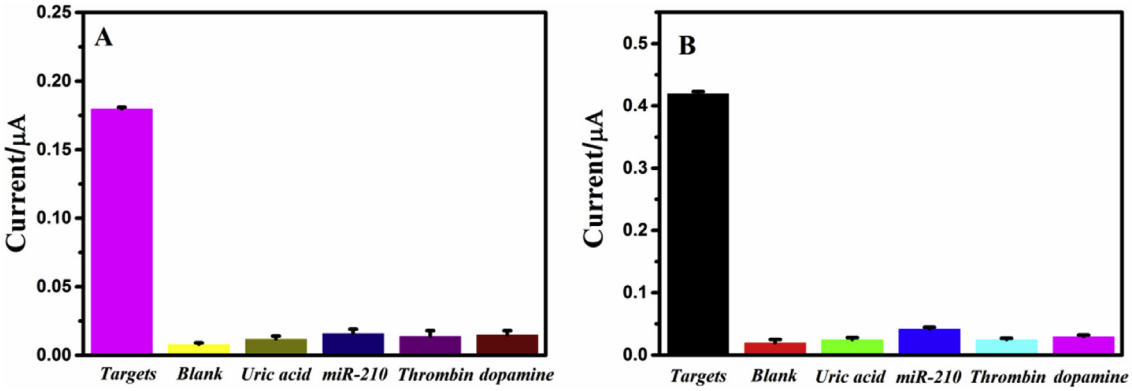

Fig. 7. Selectivity of the proposed sensor toward (A) miR-141 against blank, uric acid, miR-210 and dopamine at 1 nM and (B) miR-21 against blank, uric acid, miR-210 and dopamine at 1 nM.

Table 2
Comparison of different methods for miRNAs detection.

Target	Detection method	Detection limit	Refs.
miR-21,miR-155	ECL	1.51 fM,1.67 fM	[39]
miRNA196a, miRNA210	CV	10 fM, 10 fM	[40]
miR-21,miR-122,miR-223	SERS	2.72,0.24,2.68pM	[41]
miR-155,miR-27b	SWV	12 fM, 31 fM	[42]
miR-21,miR-141	SWV	0.1 fM, 0.1 fM	This work

some other potential coexistent species in body fluid sample such as thrombin and uric acid. As shown in Fig. 7, the current signal at MB and Fc redox potential only show negligible increase in the presence of 100 nM miR-210, 100 nM dopamine, 100 nM thrombin and 100 nM uric acid, compared to sharp increase of signal after adding 1 nM miR-141 and 1 nM miR-21. These results imply that the biosensor offered high selectivity toward miR-141 and miR-21, probably due to the highly specific hybridization between the probe DNA and target miRNA. The reproducibility was examined by cross comparison of five fabricated biosensors in the same batch. The relative standard deviations (RSD) obtained are 2.5% for 1 nM of miR-141 and 4.1% for 1 nM of miR-21, respectively, which is relatively acceptable for lab-scale production. Additionally, the stability of the biosensor was inspected that only a small decrease of the peak current was observed after 1 week of storage at 4 °C and the signal response of miR-141 and miR-21 was still retained above 90% and 89% of their initial value after four weeks of storage. The stable performance of the biosensor can be attributed to chemical stability of the sensory material components. These results suggested the biosensor is suitable for analytic application in ambient environment.

3.6. Sensing performance in practical application

Finally, to illustrate the feasibility of our sensory platform for miRNA detection in clinical environment, experiments were conducted by using the method of standard addition by adding 20, 60, 200, 600 and 1000 pM of miR-141 and miR-21 into human serum samples. As shown in Table 3, a good recovery in the range of 97.3–108% was observed for simultaneously detecting the two miRNA targets in one batch, revealing a wide detection range with less interference from the body fluid. The results indicate that our proposed sensing platform can be potentially applied to monitor miRNA in complex clinic samples.

4. Conclusion

In summary, we have reported a facile fabricated paper-based biosensor for the simultaneous detection of two clinic relevant miRNA. The hierarchical assembled nanomaterials enabled large surface area for capturing target molecule, amplifying reporter oligo hybridization events, eventually enhancing the catalytic redox signal. All of these factors contributed to outstanding sensory performance with low detection limit, high specificity and good stability. Considering the paper based nature, this platform paves the way to high performance, low cost electrochemical biosensors for point-of-care testing.

Table 3
Detection of miR-141 and miR-21 in serum samples with the proposed biosensor (n = 5).

Sample miR-141/miR-21	Added(pM) miR-141/miR-21	Found(pM) miR-141/miR-21	Recovery(%) miR-141/miR-21
1	20	20.4/20.8	104/108
2	60	59.1/60.6	98.5/101
3	200	202/201.5	101/107.5
4	600	584/592	97.3/98.7
5	1000	1006/991	100.6/99.1

Declaration of interest statement

We declare that we have no financial and personal relationships with other people or organizations that can inappropriately influence our work, there is no professional or other personal interest of any nature or kind in any product, service and/or company that could be construed as influencing the position presented in, or the review of, the manuscript entitled.

Acknowledgment

This work was supported financially by Tsinghua-Peking Joint Center for Life Sciences Post-doctoral Fund.

Appendix A. Supplementary data

Supplementary data to this article can be found online at https://doi.org/10.1016/j.aca.2019.01.036.

References

[1] H.L. Guo, N.T. Ingoia, J.S. Weissman, D.P. Bartel, MicroRNAs predominantly act to decrease target mRNA levels, Nature 466 (2010) 835–840.
[2] H.V. Tran, B. Piro, S. Reisberg, L.H. Nguyen, T.D. Nguyen, H.T. Duc, M.C. Pham, An electrochemical ELISA-like immunosensor for miRNAs detection based on screen-printed gold electrodes modified with reduced graphene oxide and carbon nanotubes, Biosens. Bioelectron. 62 (2014) 25–30.
[3] M. Lagos-Quintana, R. Rauhut, W. Lendeckel, T. Tuschl, Identification of novel genes coding for small expressed RNAs, Science 294 (2001) 853–858.
[4] W. Li, K. Ruan, MicroRNA detection by microarray, Anal. Bioanal. Chem. 394 (2009) 1117–1124.
[5] F.Y. Li, J. Peng, J.J. Wang, H. Tang, L. Tan, Q.J. Xie, S.Z. Yao, Carbon nanotube-based label-free electrochemical biosensor for sensitive detection of miRNA-24, Biosens. Bioelectron. 54 (2014) 158–164.
[6] H. Zhang, Q. Wang, X.H. Yang, K. Wang, Q. Li, Z.P. Li, L. Gao, W.Y. Nie, Y. Zheng, An isothermal electrochemical biosensor for the sensitive detection of microRNA based on a catalytic hairpin assembly and supersandwich amplification, Analyst 142 (2017) 389–396.
[7] W.Y. Zhu, X.P. Su, X.Y. Gao, Z. Dai, X.Y. Zou, A label-free and PCR-free electrochemical assay for multiplexed microRNA profiles by ligase chain reaction coupling with quantum dots barcodes, Biosens. Bioelectron. 53 (2014) 414–419.
[8] S.K. Mahadeva, K. Walus, B. Stoeber, Paper as a platform for sensing applications and other devices: a review, ACS Appl. Mater. Interfaces 7 (2015) 8345–8362.
[9] D.M. Cate, J.A. Adkins, J. Mettakoonpitak, C.S. Henry, Recent developments in paper-based microfluidic devices, Anal. Chem. 87 (2015) 19–41.
[10] A.W. Martinez, S.T. Phillips, M.J. Butte, G.M. Whitesides, Patterned paper as a platform for inexpensive, low-volume, portable bioassays, Angew. Chem. Int. Ed. 46 (2007) 1318–1320.
[11] A.W. Martinez, S.T. Phillips, E. Carrilho, S.W. Thomas III, H. Sindi, G.M. Whitesides, Simple telemedicine for developing regions: camera phones and paper-based microfluidic devices for real-time, off-site diagnosis, Anal. Chem. 80 (2008) 3699–3707.
[12] R. Pelton, Bioactive paper provides a low-cost platform for diagnostics, TrAC Trends Anal. Chem. (Reference Ed.) 28 (2009) 925–942.
[13] A.D. Anderson, M.G.C. Thiago, M.C. Rafael, C.D. Lucas, A.A.M. Rodrigo, M.R. Eduardo, K.T.C. Wendell, Paper-based enzymatic reactors for batch injection analysis of glucose on 3D printed cell coupled with amperometric detection, Sens. Actuators, B: Inside Chem. 226 (2016) 196–203.
[14] L.L. Liang, F.F. Lan, X.M. Yin, S.G. Ge, J.H. Yu, M. Yan, Metal-enhanced fluorescence/visual bimodal platform for multiplexed ultrasensitive detection of microRNA with reusable paper analytical devices, Biosens. Bioelectron. 95 (2017) 181–188.
[15] H.Y. Fu, J.H. Yang, G. Lin, J.F. Nie, QiB. Yin, L. Zhang, Y. Zhang, Using the Rubik's Cube to directly produce paper analytical devices for quantitative point-of-care aptamer-based assays, Biosens. Bioelectron. 96 (2017) 194–200.
[16] N.N. Sun, R.M. Kong, F. Qu, X. Zhang, S. Zhang, J. You, An amplified fluorescence detection of T4 polynucleotide kinase activity based on coupled exonuclease III reaction and a graphene oxide platform, Analyst 140 (2015) 1827–1831.
[17] S. Pang, S. Liu, X. Su, An ultrasensitive sensing strategy for the detection of

lead (II) ions based on the intermolecular G-quadruplex and graphene oxide, Sensor. Actuator. B Chem. 208 (2015) 415–420.
[18] J.Y. Kim, S. Byun, A.J. Smith, J. Yu, J.X. Huang, Enhanced electrocatalytic properties of transition-metal dichalcogenides sheets by spontaneous gold nanoparticle decoration, J. Phys. Chem. Lett. 4 (2013) 1227–1232.
[19] O. Parlak, A. Incel, L. Uzun, A.P.F. Turner, A. Tiwari, Structuring Au nanoparticles on two-dimensional MoS_2 nanosheets for electrochemical glucose biosensors, Biosens. Bioelectron. 89 (2017) 545–550.
[20] Y. Shi, J. Wang, C. Wang, T.T. Zhai, W.J. Bao, J.J. Xu, X.H. Xia, H.Y. Chen, Hot electron of Au nanorods activates the electrocatalysis of hydrogen evolution on MoS_2 nanosheets, J. Am. Chem. Soc. 137 (2015) 7365–7370.
[21] S. Su, M. Zou, H. Zhao, C.F. Yuan, Y.N. Xu, C. Zhang, L.H. Wang, C.H. Fan, L.H. Wang, Shape-controlled gold nanoparticles supported on MoS_2 nanosheets: synergistic effect of thionine and MoS_2 and their application for electrochemical label-free immunosensing, Nanoscale 7 (2015) 19129–19135.
[22] P. Zhang, M. Fujitsuka, T. Majima, Hot electron-driven hydrogen evolution using anisotropic gold nanostructure assembled monolayer MoS_2, Nanoscale 9 (2017) 1520–1526.
[23] S. Su, H.F. Sun, W.F. Cao, J. Chao, H.Z. Peng, X.L. Zuo, W. Yu, L.H, C.H. Fan, L.H. Wang, Dual-target electrochemical biosensing based on DNA structural switching on gold nanoparticle-decorated MoS_2 nanosheets, ACS Appl. Mater. Interfaces 8 (2016) 6826–6833.
[24] Y.Y. Yang, H. Zhang, C.S. Huang, D.P. Yang, N.Q. Jia, Electrochemical non-enzyme sensor for detecting clenbuterol (CLB) based on MoS_2-Au-PEI- hemin layered nanocomposites, Biosens. Bioelectron. 9 (2017) 461–467.
[25] S.Y. Cho, H.J. Koh, H.W. Yoo, J.S. Kim, H.T. Jung, Tunable volatile-organic compound sensor by using Au nanoparticle incorporation on MoS_2, ACS Sens. 2 (2017) 183–189.
[26] H.L. Shuai, K.J. Huang, Y.X. Chen, L.X. Fang, M.P. Jia, Au nanoparticles/hollow molybdenum disulfide microcubes based biosensor for microRNA-21 detection coupled with duplex-specific nuclease and enzyme signal amplification, Biosens. Bioelectron. 89 (2017) 989–997.
[27] A. Carne, C. Carbonell, I. Imaz, D. Maspoch, Nanoscale metal–organic materials, Chem. Soc. Rev. 40 (2011) 291–305.
[28] M. Ma, H. Noei, B. Mienert, J. Niesel, E. Bill, M. Muhler, R.A. Fischer, Y. Wang, U. Schatzschneider, N. Metzler-Nolte, Iron Metal-Organic frameworks MIL-88B and NH_2-MIL-88B for the loading and delivery of the gasotransmitter carbon monoxide, Chemistry 19 (2013) 6785–6790.
[29] K.M. Taylor-Pashow, J. Della Rocca, Z. Xie, S. Tran, W. Lin, Postsynthetic modifications of iron-carboxylate nanoscale metal-organic frameworks for imaging and drug delivery, J. Am. Chem. Soc. 131 (2009) 14261–14263.
[30] F. Luo, Y. Lin, L. Zheng, X. Lin, Y. Chi, Encapsulation of hemin in metal–organic frameworks for catalyzing the chemiluminescence reaction of the H_2O_2–luminol system and detecting glucose in the neutral condition, ACS Appl. Mater. Interfaces 7 (2015) 11322–11329.
[31] S. Xie, J. Ye, Y. Yuan, Y. Chai, R. Yuan, A multifunctional hemin@ metal–organic framework and its application to construct an electrochemical aptasensor for thrombin detection, Nanoscale 7 (2015) 18232–18238.
[32] M.T. Zhao, K. Deng, L.C. He, Y. Liu, G.D. Li, H.J. Zhao, Z.Y. Tang, Core–shell palladium nanoparticle@ metal–organic frameworks as multifunctional catalysts for cascade reactions, J. Am. Chem. Soc. 136 (2014) 1738–1741.
[33] G. Frens, Controlled nucleation for the regulation of the particle size in monodisperse gold suspensions, Nature 241 (1973) 20–22.
[34] Y.G. Sun, B. Gates, B. Mayers, Y.N. Xia, Crystalline silver nanowires by soft solution processing, Nano Lett. 2 (2002) 165–168.
[35] Q. Fu, K. Xie, S. Tan, J.M. Ren, Q. Zhao, P.A. Webley, G.G. Qiao, The use of reduced copper metal–organic frameworks to facilitate CuAAC click chemistry, Chem. Commun. 52 (2016) 12226–12229.
[36] W. Zhang, J.Y. Xie, W. Hou, Y.Q. Liu, Y. Zhou, J. Wang, One-Pot template-free synthesis of Cu-MOR zeolite toward efficient catalyst support for aerobic oxidation of 5-hydroxymethylfurfural under ambient pressure, ACS Appl. Mater. Interfaces 8 (2016) 23122–23132.
[37] L.X. Chen, W.F. Zhao, Y.F. Jiao, X.W. He, J. Wang, Y.K. Zhang, Characterization of Ag/Pt core-shell nanoparticles by UV–vis absorption, resonance light-scattering techniques, Spectrochim. Acta 68 (2007) 484–490.
[38] S. Su, W.F. Cao, W. Liu, Z.W. Lu, D. Zhu, J. Chao, L.X. Weng, L.H. Wang, C.H. Fan, L.H. Wang, Dual-mode electrochemical analysis of microRNA-21 using gold nanoparticle-decorated MoS_2 nanosheet, Biosens. Bioelectron. 94 (2017) 552–559.
[39] L. Peng, P. Zhang, Y. Chai, R. Yuan, Bi-directional DNA walking machine and its application in an enzyme-free electrochemiluminescence biosensor for sensitive detection of microRNAs, Anal. Chem. 89 (2017) 5036–5042.
[40] D. Zeng, Z. Wang, Z. Meng, P. Wang, L. San, W. Wang, A. Aldalbahi, L. Li, J. Shen, X. Mi, DNA tetrahedral nanostructure-based electrochemical miRNA biosensor for simultaneous detection of multiple miRNAs in pancreatic carcinoma, ACS Appl. Mater. Interfaces 9 (2017) 24118–24125.
[41] W. Zhou, Y.-F. Tian, B.-C. Yin, B.-C. Ye, Simultaneous surface-enhanced Raman spectroscopy detection of multiplexed microRNA biomarkers, Anal. Chem. 89 (2017) 6120–6128.
[42] W. Zhu, X. Su, X. Gao, Z. Dai, X. Zou, A label-free and PCR-free electrochemical assay for multiplexed microRNA profiles by ligase chain reaction coupling with quantum dots barcodes, Biosens. Bioelectron. 53 (2014) 414–419.